Supplementary material to: Milani et al., 'Geochemical and geochronological constraints on the Mesoproterozoic Red Granite Suite, Kunene AMCG Complex of Angola and Namibia', Precambrian Research.

Analytical techniques

1. X-ray Fluorescence (XRF)

The samples were roasted in alumina refractory crucibles at 1000°C to determine loss-on-ignition (LOI). Pressed pellets were prepared mixing 10-30 g of sample with 20 drops of Moviol (PVA) as the binder. Small containers were 2/3-filled with the mixture and pressed at 10 tons with a hydrologic jack. One gram of sample was mixed with 6 g lithiumtetraborate flux and fused at 1050°C to make a stable fused glass bead. Pressed pellets and fused beads were analyzed for major element oxides and trace elements by X-ray fluorescence (XRF) spectrometry at the Stoneman Laboratory, University of Pretoria, using a Thermo Fisher ARL Perform'X Sequential XRF instrument. Data were reduced and processed with the software Uniquant.

2. Inductively coupled plasma mass spectrometry (ICP-MS)

Twenty-one samples were analyzed in the Earth Lab, Wits University, using a Thermo Scientific iCAP RQ. 50 mg of sample was weighed and digested in an open beaker/hotplate. In this method 50 mg sample which are initially put directly into a 15 mL savilex beaker with 3 mL of Ultra High Purity 2:1 HF:HNO3 and placed on the hotplate at 70°C and allowed to evaporated off. Once dry, 3 mL of HF:HNO3 were added and capped and placed on the hotplate at 70°C for 72 hours. The sample was then dried down at 70°C and 3mL HNO3 added and evaporated off. A further 3mL HNO3 was added and the beaker capped and placed on the hotplate at 70°C for 24 hours, to facilitate acid evaporation. Three mL of HNO3 were added again and allowed to evaporate off.

The samples were diluted to 50 mL (Dilution Factor 1:1000) with 5% HNO3 with 100 ppb Re and Rh as well as 50 ppb In and Bi. These elements are Internal Standards and were monitored throughout the analyses. Fluorides were minimized by allowing minimal contact between the sample and HF while still accomplishing total digestion. Samples were visually inspected for fluorides that occur as a precipitate once diluted. Calibration Standards were prepared at 5 different concentrations (10, 30, 50, 75 and 100 ppb) with all the elements to be analyzed present (40 elements) from purchased International Certified Reference Materials.

The Thermo Scientific iCAP RQ is optimized for maximum counts on In and oxide levels set to less than 2% as well as doubly charged ions set to less than 2%. All measurements were done in triplicate by the instrument and averaged, replicate deviation greater than 2% were flagged. Certified Reference Materials BCR-1, BHVO-2 and BIR-1 were digested and analyzed with all unknowns. The CRM must show less than 10% deviation from known concentrations for all elements to pass the Quality Controls, and they were typically within 5%. A Total Procedural Blank (TPB) was analyzed with all the unknowns, by taking a blank beaker through the whole sample digestion procedure.

3. Mineral separation

The mineral separation procedure conducted for this research differed from the traditional methods in that SELFRAG technology at the Stoneman laboratory (University of Pretoria) was used to cleanly liberate grains of interest along grain boundaries, in a clean and fast process. This was followed by ultrasonication and wet sieving into several size fractions. Each size fraction was then panned to produce a heavy mineral concentrate, which was then picked. SELFRAG technology removes the need to crush and mill the sample, produces very few fines, and ensures particularly good recovery of any heavy minerals. In most cases a much smaller amount of sample is required to recover a suitable quantity of grains. A major benefit is that the shape and hardness of the minerals of interest are not a factor in their liberation, therefore brittle flat crystals and soft grains can be liberated together with more resilient grains such as zircon.

All rocks were first reduced in size to fit the processing vessel of the SELFRAG (i.e., approximately 4cm x 2cm x 1cm). Thereafter the SELFRAG high voltage pulsed power instrument was used to liberate minerals of interest from each rock sample. The liberation of minerals by high voltage electrical pulses happens through the localisation of multiple electrical breakdowns along the interfaces (grain boundaries) of the different mineral phases, which causes them to separate. These grain boundaries include pre-existing cracks and alterations so that liberated grains are typically monomineralic and clean. The SELFRAG process does not reduce the entire sample to less than a certain grain size but liberates the minerals of interest.

The most effective way to separate heavy minerals was to sieve the resultant disaggregated sample into several size fractions. In addition, the size range of the heavy minerals of interest was limited to a discrete size range, so sieving assists in concentrating them, enabling easier separation. A range of size fractions were collected (in microns): -32, +32-50, +50 -63, +63 -90, +90 -125, +125 -250, +250 -300, +300 -355, +355 -500, +500 -2000. Most heavy minerals for geochronology tend to occur in a subset of these fractions, depending on their grain size, and four sequential size fractions were processed further, based on what is found and in which fraction. The sieving of the sample was performed wet, after ultrasonication, to ensure that the entrained smaller material in each fraction was minimised, and to remove any adhering clay particles to ensure ultra-clean grains.

Each size fraction selected for further examination was then panned. Due to the highly effective pre-concentration of heavy minerals by preferential liberation, and most matrix minerals being coarser-grained, the amount of material per size fraction was relatively small compared to the original sample amount. This made panning a fast and effective method to produce a heavy mineral concentrate. For more effective panning, ethanol was used instead of water. This works well in smaller size fractions, as it minimises the floatation of grains due to reduced surface tension.

After panning, the concentrate for each size fraction was placed separately on clean glass slides and examined under a stereomicroscope. Grains of interest were then picked and placed on clean glass slides. The glass slides were prepared by placing a 25 mm square of Kapton polyimide double-sided tape at one end, with a 5 mm x 25 mm strip of tape in the centre of the other half. The square of tape was then

subdivided into four quarters by marking the underside with a permanent marker. Each quarter provides a space for the picked grains of a specific size fraction.
The slide with the concentrate for a specific size fraction was then placed next to the prepared slide for picking. Picking was done using a fine-pointed pair of tweezers. A skilled picker can pick and place grains down to 10 to 15 microns. The grains were placed in regular arrays. Grains with different appearances were placed in separate arrays. In terms of appearance, the shape, colour, lustre, inclusions, etc. were considered. At least 10 grains of each type were picked and placed for identification.
After optical screening, representative grains were selected for detailed characterization by scanning electron microscopy (SEM), backscattered electron (SEM-BSE), and cathodoluminescence (SEM-CL) using a Tescan Vega 3 electron microscope equipped with a (Li)Si X-ray detector at the Spectrum Centre of the University of Johannesburg.

4. U-Pb geochronology

U-Pb age data were determined using a Nu Plasma II multi-collector inductively coupled plasma mass spectrometer (MC-ICPMS; Nu Instruments, Wrexham) housed in the Spectrum Analytical facility at the University of Johannesburg. The instrument is equipped with 16 Faraday detectors and 5 ion counting detectors, and was coupled to an ASI Resonetics 193 nm ArF RESOlution SE Excimer laser ablation system (Australian Scientific Instruments, Fyshwick). An RF power of 1300W, a coolant gas flow of 13 L/min, an auxiliary gas flow of 0.80 L/min, and a nebulizer gas flow of 0.9 L/min were used for analyses. The reflected power was less than 3W. The He laser carrier gas flow was 0.3 L/min. The detector configuration for U-Pb measurements were as follow: H8 = ^{238}U; H7 = ^{232}Th; IC0 = ^{208}Pb; IC1 = ^{207}Pb; IC2 = ^{206}Pb; IC3 = ^{204}Pb (+ ^{204}Hg); IC4 = ^{202}Hg.
Zircon grains were imaged under a SEM-based cathodoluminescence source prior to analysis. Spot laser ablations of 30 μm were performed, using a laser energy of 4 to 6 mJ, at a frequency of 2 Hz, and at 25% transmittance. The resulting fluence was ~1.2 J.cm^{-2}. The 50 second sample ablations were preceded by a 20 second blank measurement. Instrumental mass bias and fractionation was corrected through sample-standard bracketing, and all corrections and other calculations were performed off-line using an inter-active excel spreadsheet program as described by Andersen et al. (2009). Zircon reference samples GJ1 (^{207}Pb/^{206}Pb age = 609 ± 1 Ma; Belousova et al., 2005), 91500 (^{207}Pb/^{206}Pb age = 1065 ± 1 Ma; Wiedenbeck et al., 1995) and A382 (^{207}Pb/^{206}Pb age = 1877 ± 2 Ma; Huhma et al., 2012) were used as calibration standards, and CDQGNG (1842.0 ± 3.1 Ma; Black et al., 2003) was used as a secondary reference material. Some of the dates where the zircon grains plot on a discordia have very few zircons plotting on the concordia, and for them we preferred not to report the weighted mean, considering the discordant age as more reliable. Therefore, we chose to report the concordant (or discordant) date for all rocks, and the ^{207}Pb/^{206}Pb weighted mean when available.
Results for 44 spot measurements of the secondary reference material CDQGNG, measured over several analytical sessions, producing a weighted mean ^{207}Pb/^{206}Pb age of 1842.6 ± 1.4 Ma (MSWD = 3.7; n = 54/56, Fig. 1). Secondary standard analyses with discordance greater than 5% were discarded. Weighted

mean $^{207}Pb/^{206}Pb$ ages and concordia dates were calculated and presented using the IsoplotR open source software (Vermeesch, 2018) and Isoplot software (Ludwig, 2003), respectively.

Zircon habits and textures

Zircons range in size from 50 to 500 μm. Xenocrystic cores and recrystallization rims are typically absent. The grain shapes are quite variable among the samples, ranging from near-euhedral, prismatic with well-preserved oscillatory zoning, to anhedral/stubby grains with complex multiple oscillatory zoning domains, to embayed grains with patchy textures, fractures and dark to very dark metamict areas. The latter were not suitable for dating. In some cases (e.g., KAC226-224), no datable grains could be separated. BSE and CL images revealed that many grains underwent possible radiation damage, and these were still mounted and analyzed to get reasonable statistics on the age of each sample. All the obtained concordant ages are verified at the >95% level of confidence.

Red Granite Suite

KAC186-188: zircons are mostly subhedral, 50-150 μm in size, and show complex patchy or sector zoning with fracturing and metamictization (U often exceeding 1000 ppm).

KAC269-269: in CL images, zircons appear as stubby tabular grains, 50-200 μm in size. The original zoning has been replaced by patchy textures. Fractured grains are common, with concentric cracks expanding radially to the outer zone.

KAC260-254: in CL images, tabular zircons (of 100-300 μm in size) preserve rare oscillatory zoning and show dark and fractured patches due to partial radiation damage. Outer rims indicating resorption and reprecipitation during magmatic overgrowth are visible in some grains.

KAC61-58: in CL images, zircon is euhedral to subhedral, between 200 and 500 μm long, and many have well-preserved fine oscillatory zoning.

KAC301-1: Zircons typically do not exceed 100 μm and are mostly subhedral. Some grains preserve regular concentric oscillatory zoning, whereas in others, zoning is disrupted by irregular bright non-homogenous patchy zones, possibly caused by subsolidus modification.

KAC297: in CL images, zircon is prismatic, typically fragmented, and is typically 100 to 200 μm in size. Resorption zones with bright cloudy areas of reprecipitation are common and distinct zoning is visible in a few crystals.

KAC274: CL images show dark and largely fragmented zircons, rarely exceeding 100 μm in size, with faint zoning patterns visible. Metamict grains are dominant, with U contents exceeding 5000 ppm. A small number of zircons show a brighter appearance with well-preserved oscillatory zoning.

Regional Granite and anorthosite KSAT35-22

KAC119-109: zircons (100-200 μm) typically show bright undifferentiated cloudy nuclei with fine outer oscillatory-zoned bands. Euhedral to subhedral inclusions of apatite (bright) and monazite have been observed.

KAC98-92: zircons (200-450 μm) are prismatic and have regular zoning.

KAC74-71: zircons (200 to 400 μm) are prismatic and are oscillatory zoned.
KAC254-250: zircons (100-300 μm) are typically prismatic and have both regularly zoned and homogeneous cloudy grains.
KSAT35-22: two large subhedral zircons with distinct oscillatory zoning (in-situ analysis).

5. Lu-Hf geochronology

Lu-Hf isotope ratio measurements were also performed using the 193nm ArF RESOlution SE excimer laser, connected to the Nu Plasma II MC-ICPMS instrument, at the University of Johannesburg. Instrumental operating conditions were similar as described for U-Pb age determinations.
Lu-Hf measurements were done during two separate sessions. Spots of 45-80 μm diameter were ablated, depending on the sizes of the zircon grains. A repetition rate of 7 Hz at 50% beam transmission was used. During the first measurement session a laser energy of 4mJ was used resulting in an on-sample fluence of 3 J/cm^2; during the second measurement session an energy of 6 mJ was used delivering 5 J/cm^2 fluence. Detector configuration was as follow: H4 = ^{180}Hf; H3 = ^{179}Hf; H2 = ^{178}Hf; H1 = ^{177}Hf; Ax = ^{176}Hf + ^{176}Yb + ^{176}Lu; L1 = ^{175}Lu; L2 = ^{174}Hf + ^{174}Yb; L3 = ^{173}Yb; L4 = ^{172}Yb; L5 = ^{171}Yb.
Results were processed using the NPII NICE data editor. Background was measured on peak for 25 seconds prior to ablation, and subtracted from the ablation signal, which lasted for 70 seconds. Background-corrected ^{171}Yb and ^{173}Yb were used to calculate a mass bias correction factor for Yb according to the Russel equation, using an accepted ^{171}Yb/^{173}Yb value of 1.12346. ^{171}Yb was then used to calculate ^{174}Yb using a ^{174}Yb/^{171}Yb ratio of 2.21559, and also to calculate ^{176}Yb using a ^{176}Yb/^{171}Yb ratio of 0.88395. Mass bias for Lu was assumed to be the same as for Yb. ^{175}Lu was used to calculate ^{176}Lu, using ^{176}Lu/^{175}Lu = 0.02645 (Thirlwall and Anczkiewicz, 2004). ^{176}Yb and ^{176}Lu were then stripped from the total signal on mass 176 to obtain ^{176}Hf, and ^{174}Yb was stripped from the signal at mass 174 to obtain ^{174}Hf. The Hf mass bias correction factor was determined from the observed ^{179}Hf/^{177}Hf, assuming a true ratio of 0.7325 (Thirlwall and Anczkiewicz, 2004). Zircon standard Temora 2 was used to evaluate the accuracy of the measurements, obtaining ^{176}Hf/^{177}Hf = 0.282679 ± 38 (2SD) vs 0.282686 ± 8 (2SD) reported by Woodhead and Hergt (2005). An average ^{174}Hf/^{177}Hf = 0.008657 ± 57 (2SD), and an average ^{178}Hf/^{177}Hf = 1.46721 ± 11 (2SD), were calculated for all sample measurements, which are comparable to the values given by Thirlwall and Anczkiewicz (2004) for these invariant ratios.
Initial ^{176}Hf/^{177}Hf and εHf were calculated using the ^{207}Pb/^{206}Pb age obtained by LA-ICP-MS dating in this work and in Lehmann et al. (2020), assuming CHUR = ^{176}Lu/^{177}Hf = 0.0336, and ^{176}Hf/^{177}Hf = 0.282785 (Bouvier et al., 2008). Model ages were calculated (in Ga) through a two-stage model using the measured ^{176}Lu/^{177}Hf of each spot (first stage = age of zircon), a value of 0.0113 for the average continental crust (second stage), and an average MORB (DM) with ^{176}Lu/^{177}Hf and ^{176}Hf/^{177}Hf of 0.0384 and 0.28314, respectively.

Supplementary material

Figures

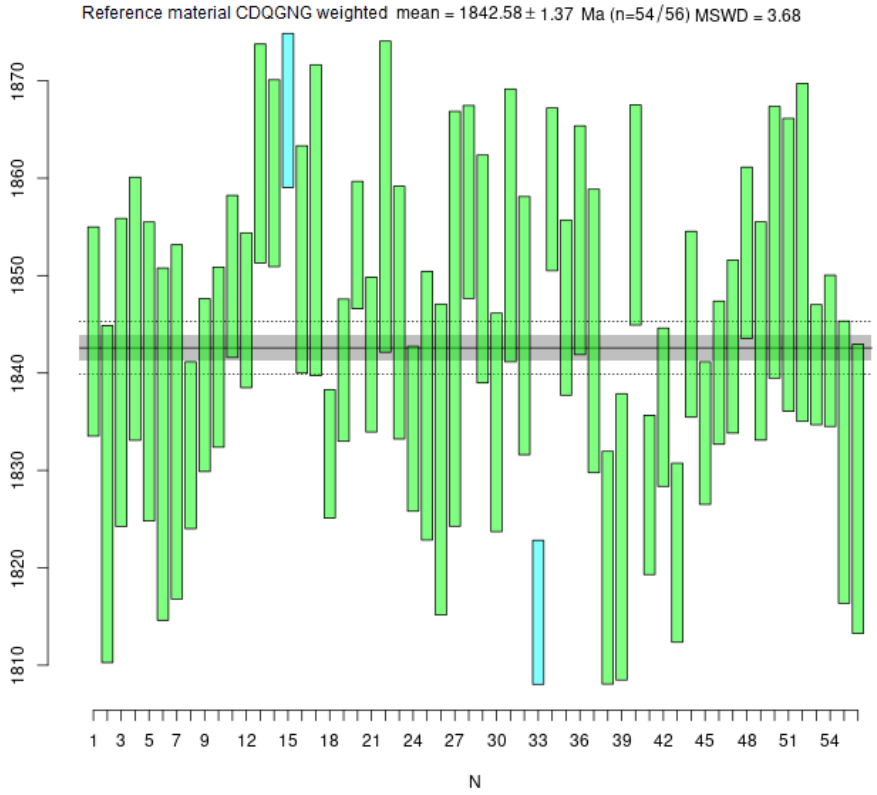

Fig. 1. $^{207}Pb/^{206}Pb$ date of reference material CDQGNG, giving an age of 1842.6 ± 1.4 Ma on 54 lines.

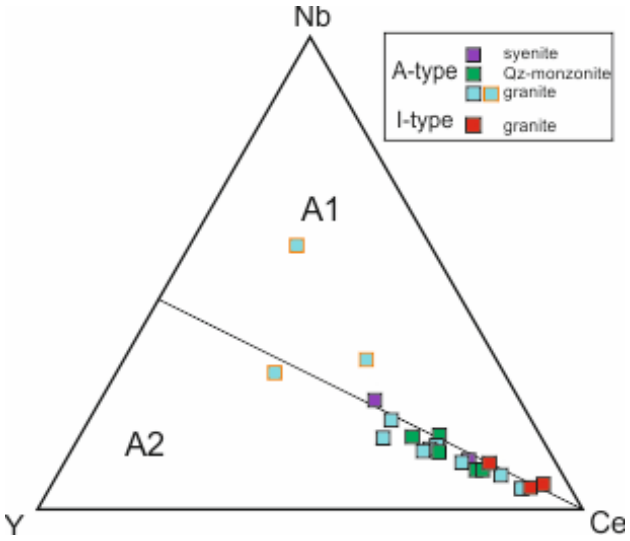

Fig. 2. Nb–Y–Ce triangular plot (Eby, 1992). A1 field refers to granitoids in anorogenic settings, A2 to post-orogenic granites emplaced after a continental collision.

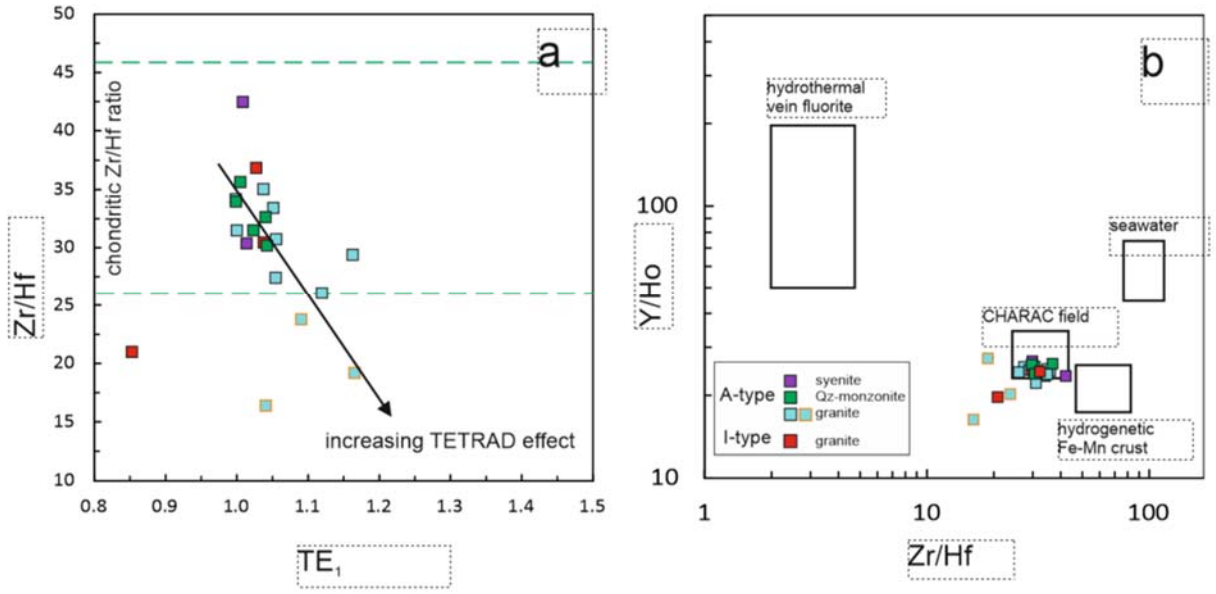

Fig. 3 a) Variation of Zr/Hf as a function of the tetrad degree (TE_1 of Irber, 1999). TE_1 is defined as (Ce/Ce* x Pr/Pr*)$^{0.5}$, with Ce/Ce*=$Ce_{(N)}/(La_{(N)}^{2/3} \times Nd_{(N)}^{1/3})$, and Pr/Pr*=$Pr_{(N)}/(La_{(N)}^{2/3} \times Nd_{(N)}^{1/3})$. Chondrite range is shown for comparison. b) Y/Ho vs. Zr/Hf ratios for the Red Granite Suite rocks. The three granites with REE tetrad effect (plus KAC43-45) plot outside the CHARAC (CHArge-and-Radius-Controlled) field (modified from Bau, 1996).

References

Andersen, T., Andersson, U.B., Graham, S., Aberg, G., Simonsen, S.L., 2009. Granitic magmatism by melting of juvenile continental crust: new constraints on the source of Palaeoproterozoic granitoids in Fennoscandia from Hf isotopes in zircon. Journal Geological Society, London 166, 233–247.

Bau, M., 1996. Controls on the fractionation of isovalent trace elements in magmatic and aqueous systems: evidence from Y/ Ho, Zr/Hf, and lanthanide tetrad effect. Contributions to Mineralogy and Petrology 123, 323-333.

Belousova E.A., Griffin W.L., O'Reilly S.Y., 2005. Zircon crystal morphology, trace element signatures and Hf isotope composition as a tool for petrogenetic modelling: examples from Eastern Australian granitoids. Journal of Petrology 47, 329-353.

Black L.P., Kamo S.L., Williams I.S., Mundil R., Davis D.W., Korsch R.J., Foudoulis, C., 2003. The application of SHRIMP to Phanerozoic geochronology; a critical appraisal of four zircon standards. Chemical Geology 200, 171-188.

Bouvier, A., Jeffrey, D., Vervoort, J.D., Patchett, P.J., 2008. The Lu–Hf and Sm–Nd isotopic composition of CHUR: constraints from unequilibrated chondrites and implications for the bulk composition of terrestrial planets. Earth and Planetary Science Letters 273, 48–57.

Eby, G.N., 1992. Chemical subdivision of the A-type granitoids: petrogenetic and tectonic implications. Geology 20, 641–644.

Huhma H, Mänttäri I, Peltonen P, Kontinen A, Halkoaho T, Hanski E, Hokkanen T, Hölttä P, Juopperi H, Konnunaho J., Layahe Y., Luukkonen E., Pietikäinen K., Pulkkinen A., Sorjonen-Ward P., Vaasjoki M., Whitehouse, M., 2012. The age of the Archaean greenstone belts in Finland. Geological Survey of Finland, Special Paper 54, 74-175.

Irber, W., 1999. The lanthanide tetrad effect and its correlation with K/Rb, Eu/Eu*, Sr/Eu, Y/Ho, and Zr/Hf of evolving peraluminous granite suites. Geochimica et Cosmochimica Acta 63, 489–508.

Lehmann, J., Bybee, G.M., Hayes, B., Owen-Smith, T.M., Belyanin, G., 2020. Emplacement of the giant Kunene AMCG complex into a contractional ductile shear zone and implications for the Mesoproterozoic tectonic evolution of SW Angola. International Journal of Earth Sciiences doi.org/10.1007/s0053 1-020-01837 -5

Ludwig, K., 2003. Isoplot/Ex version 3: A Geochronological Toolkit for Microsoft Excel. Geochronology Center, Berkeley.

Thirlwall, M.F., Anczkiewicz, R., 2004. 'Multidynamic isotope ratio analysis using MC-ICP-MS and the causes of secular drift in Hf, Nd and Pb isotope ratios', International Journal of Mass Spectrometry 235(1), 59–81.

Vermeesch, P., 2018. IsoplotR: A free and open toolbox for geochronology. Geoscience Frontiers, 9(5), 1479–1493.

Wiedenbeck M, Allé P, Corfu F, Griffin WL, Meier M, Oberli F, et al., 1995. Three natural zircon standards for U-Th-Pb, Lu-Hf, trace element and REE analyses. Geostandards Newsletter 19, 1-23.

Woodhead, J.D., Hergt, J.M., 2005. A preliminary appraisal of seven natural zircon reference materials for in situ Hf isotope determination. Geostandards and Geoanalytical Research 29(2), 183–195.